Supporting Information

Relationship between spatially heterogeneous reaction dynamics and photochemical kinetics in single crystals of anthracene derivatives

Sogo Kataoka,[a] Daichi Kitagawa,*[a] Hikaru Sotome,[b] Syoji Ito,[b] Hiroshi Miyasaka,[b] Christopher J. Bardeen,*[c] and Seiya Kobatake*[a]

[a]Department of Chemistry and Bioengineering,
Graduate School of Engineering, Osaka Metropolitan University
3-3-138 Sugimoto. Sumiyoshi-ku
Osaka, 558-8585 (Japan)

[b]Division of Frontier Materials Science and Center for Promotion of Advanced Interdisciplinary Research, Graduate School of Engineering Science, Osaka University
1-3 Machikaneyama-cho, Toyonaka, Osaka 560-8531 (Japan)

[c]Department of Chemistry
University of California, Riverside
501 Big Springs Road
Riverside, CA 92521 (USA)

*E-mail: kitagawa@omu.ac.jp; christob@ucr.edu; kobatake@omu.ac.jp

Table of Contents for supporting videos.

Movie S1. Associated with Figure 2a.

Movie S2. Associated with Figure 2b.

Movie S3. Associated with Figure 2c.

Movie S4. Associated with Figure 2d.

Movie S5. Fluorescence intensity change of **9MA** single crystal

Movie S6. Fluorescence intensity change of **9AcA** single crystal

Movie S7. Fluorescence intensity change of **9CA** single crystal

Movie S8. Fluorescence intensity change of **9AA** single crystal

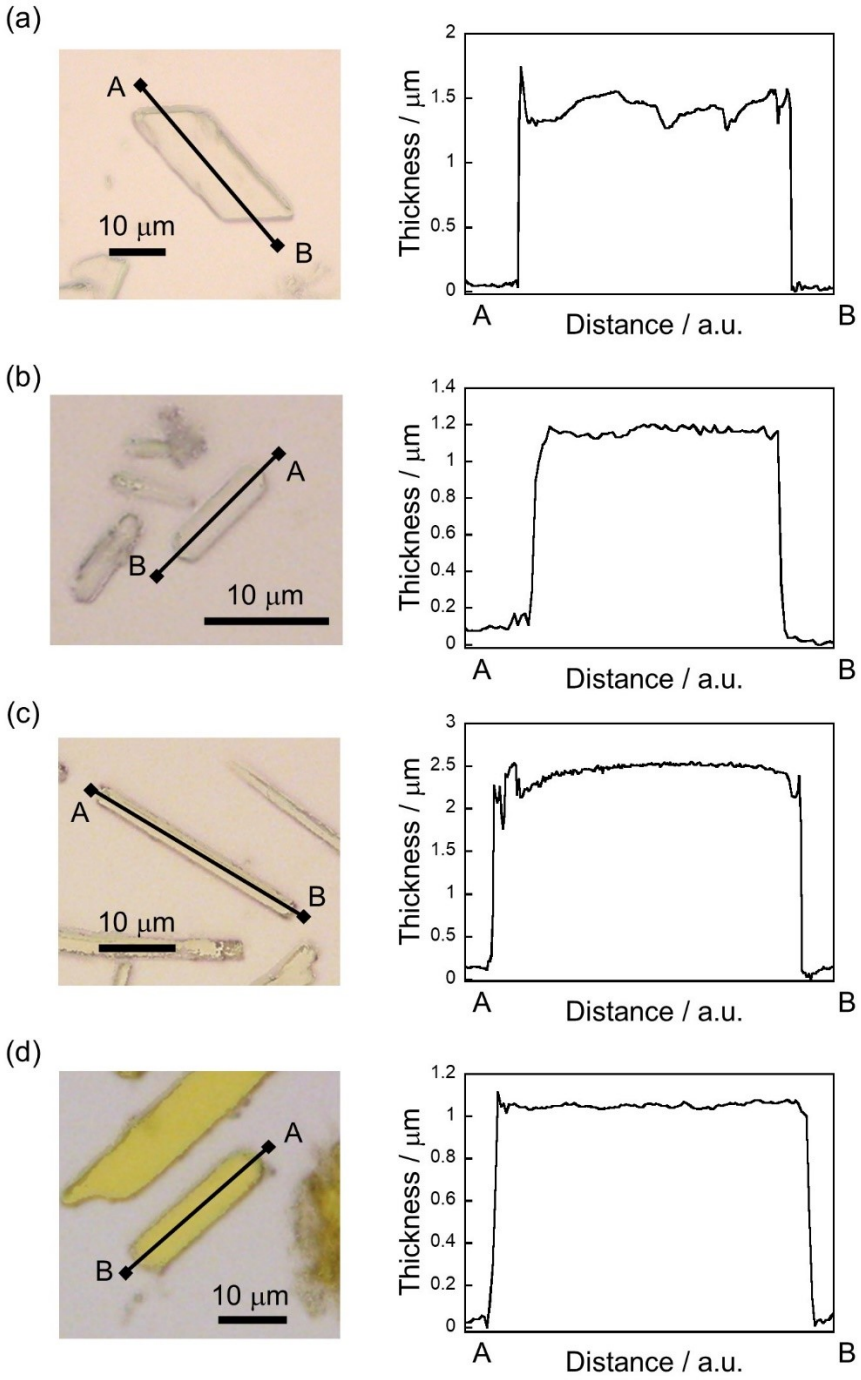

Fig. S1. Profiles of crystal thickness for (a) **9MA**, (b) **9AcA**, (c) **9CA**, and (d) **9AA**.

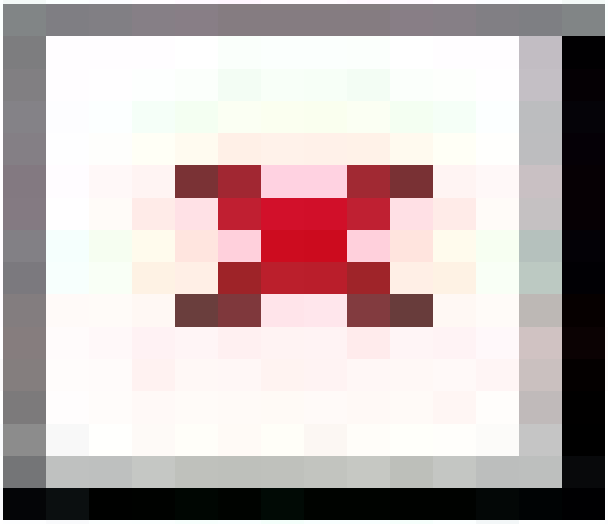

Fig. S2 PXRD pattern calculated from single crystal X-ray crystallographic data (black line), the pattern of powder crystals (red line), and the pattern of single crystals (blue line) for (a) **9MA**, (b) **9AcA**, (c) **9CA**, and (d) **9AA**.

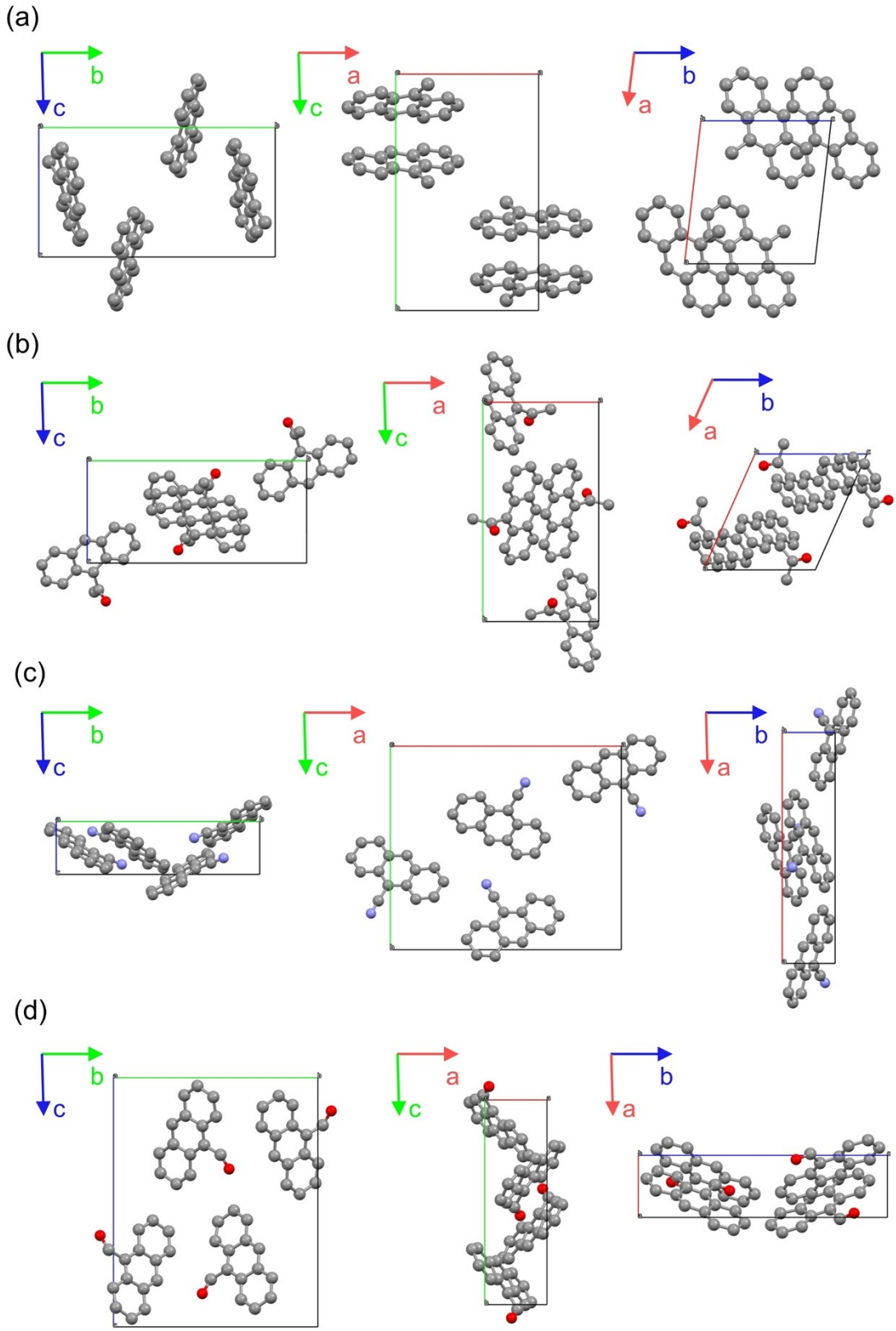

Fig. S3 Molecular packing diagrams for crystals of (a) **9MA**, (b) **9AcA**, (c) **9CA**, and (d) **9AA**.

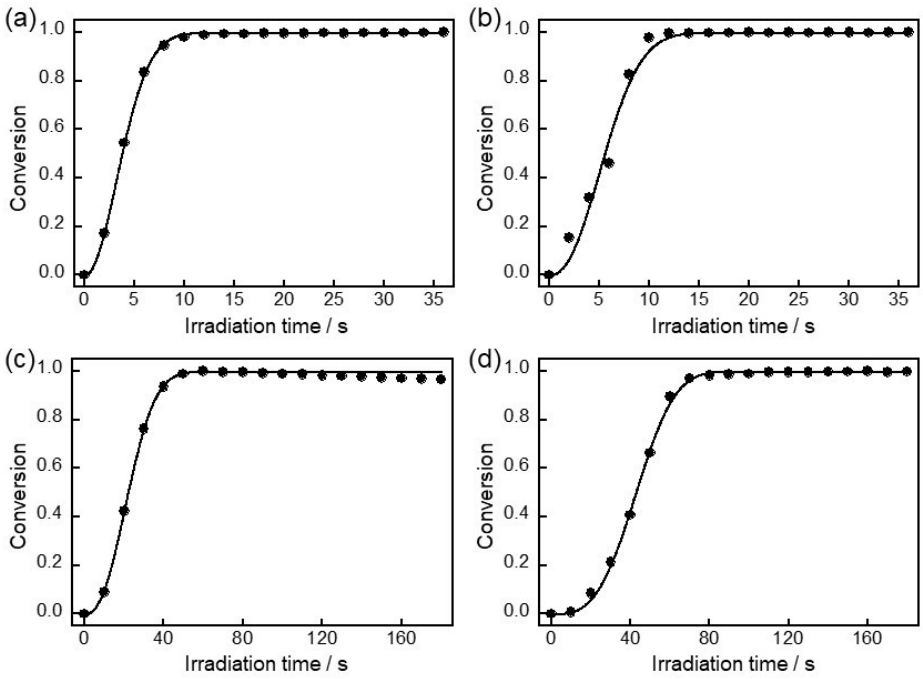

Fig. S4 Fitting of the change in conversion calculated from absorbance decay profiles of (a) **9MA** (sample 1), (b) **9AcA** (sample 4), (c) **9CA** (sample 7), and (d) **9AA** (sample 10) using Eq. (1).

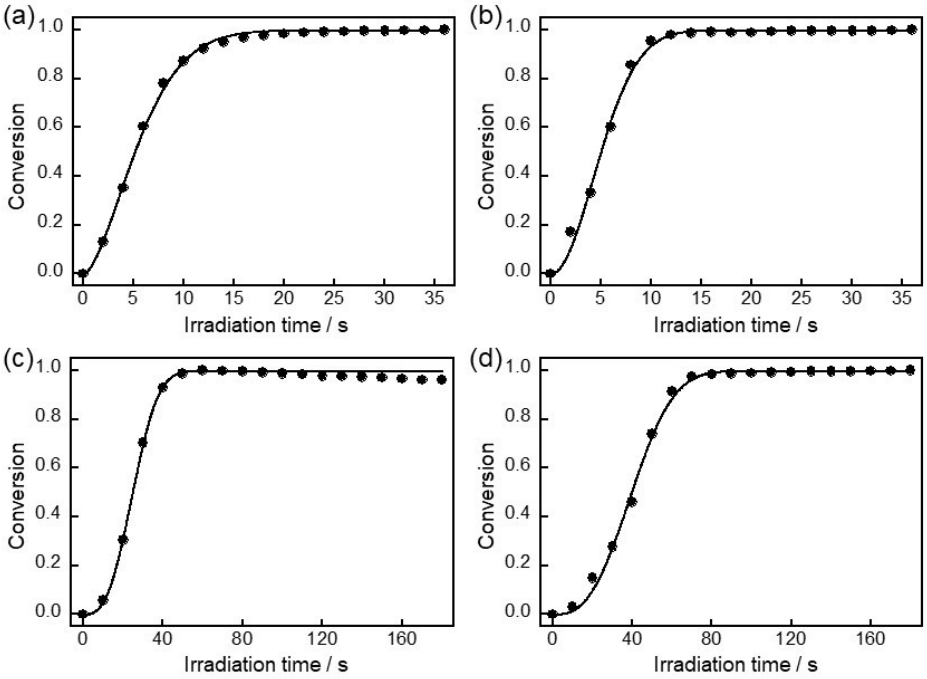

Fig. S5 Fitting of the change in conversion calculated from absorbance decay profiles of (a) **9MA** (sample 2), (b) **9AcA** (sample 5), (c) **9CA** (sample 8), and (d) **9AA** (sample 11) using Eq. (1).

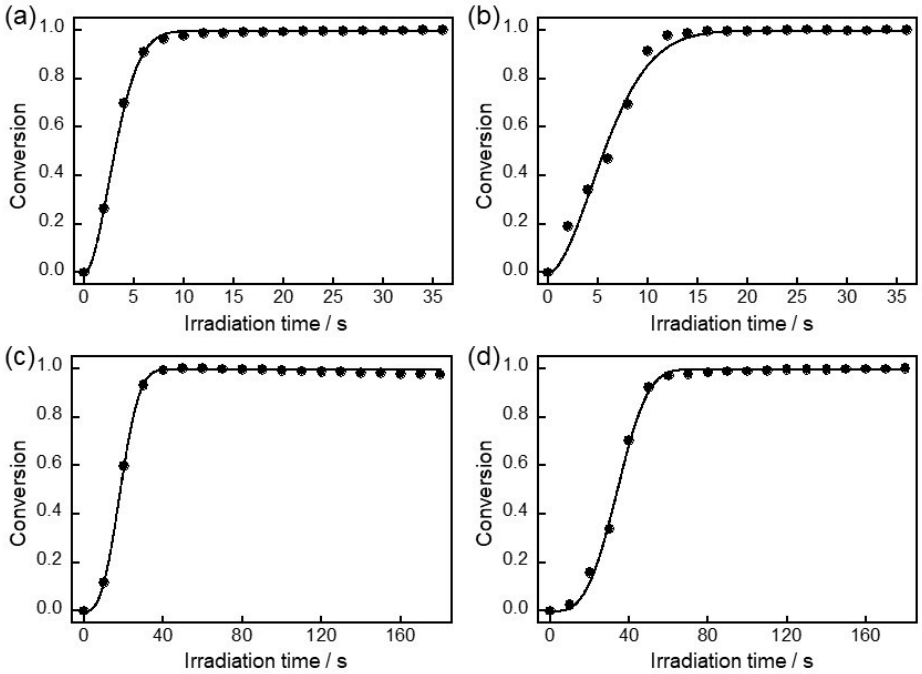

Fig. S6 Fitting of the change in conversion calculated from absorbance decay profiles of (a) **9MA** (sample 3), (b) **9AcA** (sample 6), (c) **9CA** (sample 9), and (d) **9AA** (sample 12) using Eq. (1).

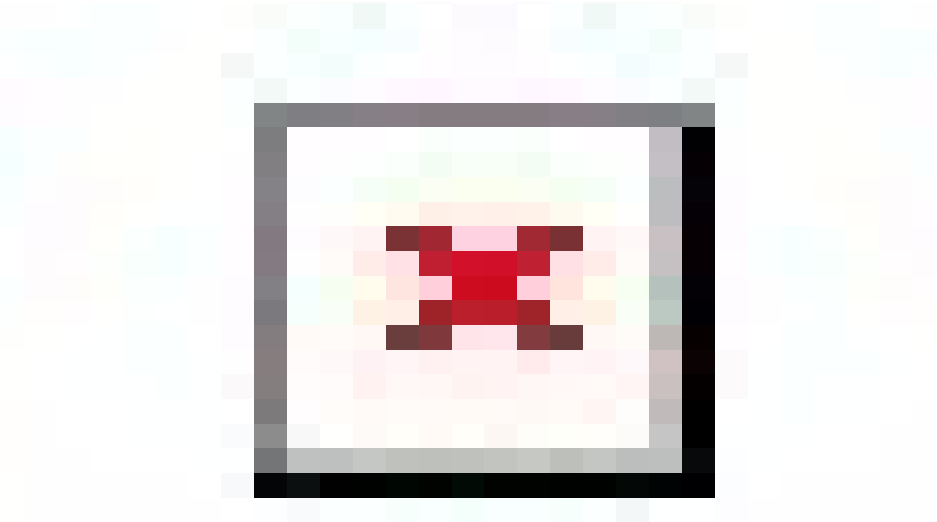

Fig. S7 Fitting of the absorbance decay profiles of (a) **9MA** (sample 1), (b) **9AcA** (sample 4), (c) **9CA** (sample 7), and (d) **9AA** (sample 10) using Eq. (3).

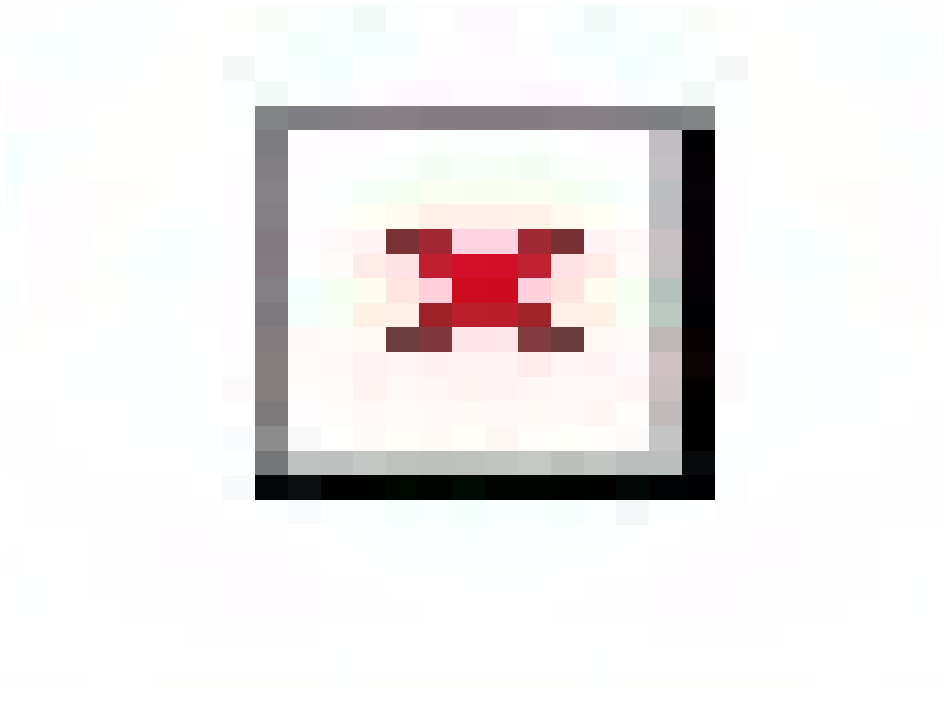

Fig. S8 Fitting of the absorbance decay profiles of (a) **9MA** (sample 2), (b) **9AcA** (sample 5), (c) **9CA** (sample 8), and (d) **9AA** (sample 11) using Eq. (3).

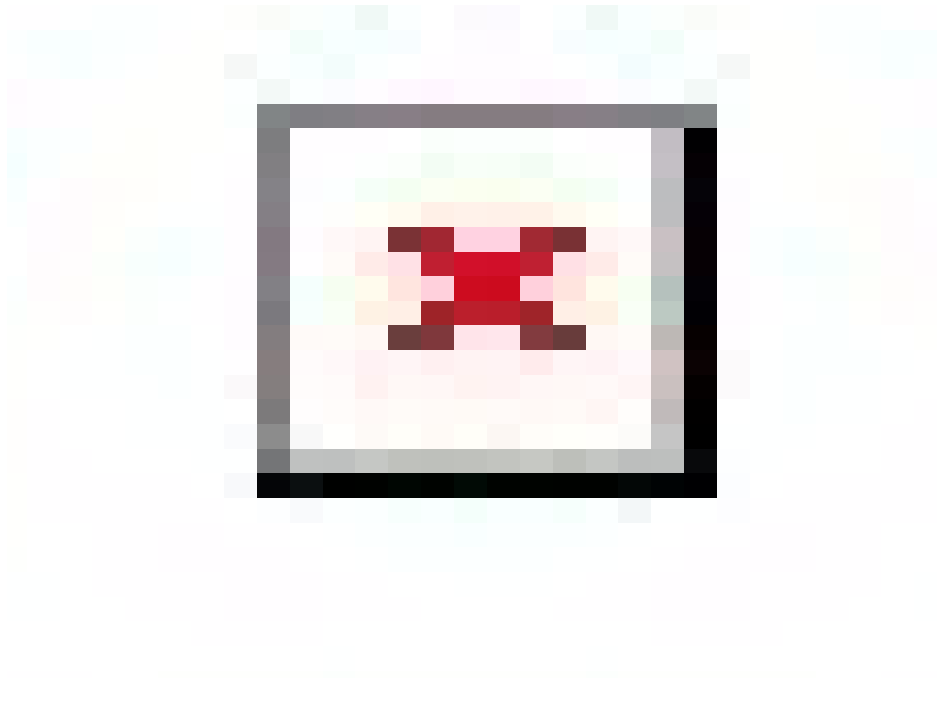

Fig. S9 Fitting of the absorbance decay profiles of (a) **9MA** (sample 3), (b) **9AcA** (sample 6), (c) **9CA** (sample 9), and (d) **9AA** (sample 12) using Eq. (3).